Energy & Environmental Science

Accepted Manuscript

This article can be cited before page numbers have been issued, to do this please use: Y. Yang, C. Liu, A. Mahata, M. Li, C. Roldán Carmona, Y. Ding, Z. Arain, W. Xu, Y. Yang, P. Schouwink, A. Züttel, F. De Angelis, S. Dai and M. K. Nazeeruddin, *Energy Environ. Sci.*, 2020, DOI: 10.1039/D0EE01833C.

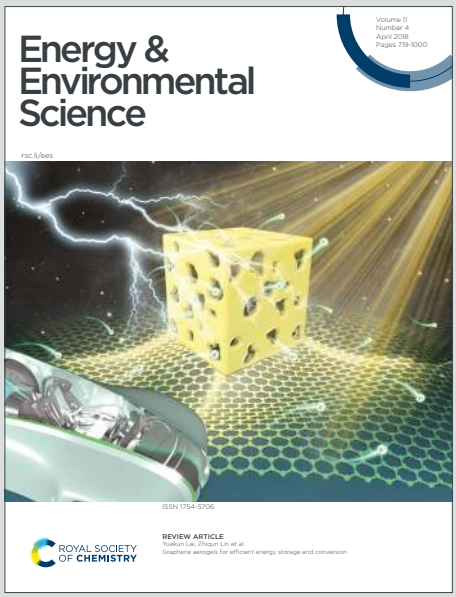

ROYAL SOCIETY OF CHEMISTRY

rsc.li/ees

View Article Online
DOI: 10.1039/D0EE01833C

Universal Approach toward High-efficiency Two-dimensional Perovskite Solar Cells via Vertical-Rotation Process

Yi Yang,[1,2†] Cheng Liu,[1,2†] Arup Mahata,[3,4] Mo Li,[2,5] Cristina Roldán-Carmona,[2] Yong Ding,[1,2] Zulqarnain Arain,[1] Weidong Xu,[1] Yunhao Yang,[1] Pascal Alexander Schouwink,[2] Andreas Züttel,[2,5] Filippo De Angelis,[3,4,6,7] Songyuan Dai[1*] and Mohammad Khaja Nazeeruddin.[2*]*

[1]Beijing Key Laboratory of Novel Thin-Film Solar Cells, Beijing Key Laboratory of Energy Safety and Clean Utilization, North China Electric Power University, Beijing 102206, P. R. China.

[2]Institute of Chemical Sciences and Engineering, EPFL Valais, 1951, Sion, Switzerland.

[3]CompuNet, Istituto Italiano di Tecnologia, Via Morego 30, 16163 Genova, Italy.

[4]Computational Laboratory for Hybrid/Organic Photovoltaics (CLHYO) Istituto CNR di Scienze e Tecnologie Chimiche "Giulio Natta" (CNR-SCITEC) Via Elce di Sotto 8, 06123 Perugia, Italy.

[5]Empa Materials Science and Technology, CH-8600 Dübendorf, Switzerland.

[6]Department of Chemistry, Biology and Biotechnology, University of Perugia, Via Elce di Sotto 8, 06123 Perugia, Italy.

[7]Chemistry Department, College of Science, King Saud University, Riyadh, Saudi Arabia.

†These authors contributed equally to this work.

[*]**Corresponding Author**

DOI: 10.1039/D0EE01833C

E-mail: dingy@ncepu.edu.cn, sydai@ncepu.edu.cn and mdkhaja.nazeeruddin@epfl.ch

Abstract: The emerging 2D perovskites exhibit superior stability and similar optoelectronic attributes compared to 3D analogous, but their strong exciton-binding energy and inferior interlayer charge-transport reduce dramatically the device performance. Herein, we report a universal approach towards high-efficiency 2D perovskite solar cells (PSCs) by using the synergistic effect of NH_4Cl and H_2O to rotate the crystallographic orientation of 2D systems. The preferential adsorption of NH_4Cl to the (202) crystal plane and the accelerated deprotonation of NH_4^+ by H_2O guide the crystal growth of the 2D framework towards vertical out-of-plane orientation, which strongly improves the 2D crystallinity, charge mobility, and carrier lifetime. As a representative, $(PEA)_2(MA)_3Pb_4I_{13}$-based PSCs ($n \leq 4$) prepared *via* the vertical-rotation process achieve a champion power conversion efficiency (PCE) of 17.03%, among the best PCEs reported for 2D PSCs. These findings offer a universal approach to rotate the orientation of 2D perovskites for efficient photovoltaics regardless of perovskite composition.

Introduction

The performance of organic-inorganic hybrid halide perovskite solar cells (PSCs) has dramatically developed to over 25% in a short time-period[1-3] increasingly approaching the Shockley-Queisser limit for a single-junction solar cell.[4] However, their significant degradation under humidity, heat, and light soaking becomes more and more prominent and intractable, which is at present the main bottleneck to impede their commercialization. Previous studies demonstrate that the degradation of three-dimensional (3D) perovskite is primarily a surface and/or interface-initiated process that gradually progress toward the bulk material, deteriorated by the heat stress above the tetragonal-cubic transition temperature.[5] Efforts towards surface functionalization, interface modification, engineering of dopant-free hole transport materials (HTMs), and crystal-defect suppression have been made to overcome their poor stability.[6-9] Recently, more promising stability has been demonstrated by the low-dimensional

Ruddlesden-Popper (LDRP) or Dion-Jacobson (LDDJ) perovskites, which possess higher structure stability and suppressed surface moisture intrusion compared to those of traditional 3D perovskites.[10,11] These perovskites are generally formed by substituting the small organic cations with bulkier cations, such as n-butylammonium (BA^+)[10,12] and 2-phenyl-ethylammonium (PEA^+)[13,14] for LDRP perovskite, or di-ammonium cations for the LDDJ perovskite.[15] As the large organic cations cannot fit into the inorganic Pb-I framework (e.g., PbI_6^{4-}), they intercalate between the inorganic sheets, forming a layered two-dimensional (2D) or quasi-2D system. The general formula of a LDRP and LDDJ perovskite is $(R)_2A_{n-1}Pb_nX_{3n+1}$ and $DA_{n-1}Pb_nX_{3n+1}$ respectively, where *R* is a large univalent cation, *A* is a small univalent cation, *D* is a divalent organic cation, *X* denotes a halide ion, and *n* stands for the number of inorganic slabs separated by the large cations. Thanks to the hydrophobic nature of these bulkier organic cations, they can effectively block the surface water adsorption and provide remarkable long-term stability compared to the 3D analogues. Besides, the van der Waals interactions between the organic layers increase the desorption energy of volatile organic components, further enhancing the stability under external stresses.[16,17] However, their strong insulating character provokes the formation of multi-quantum-wells (QWs), where the organic dielectric layers behave as charge transport barriers, and the inorganic sheets correspond to the wells.[18] This results in a dielectric confinement producing higher permittivity, larger exciton-binding energy and inhibited charge transport between the two adjacent conducting layers.[19] Therefore, reducing the materials dimension inevitably weakens the carrier transport, and sacrifices the efficiency of PSCs.[20]

To overcome the poor charge transport, two main approaches have been proposed in literature. The prior consists on increasing the number of inorganic sheets (*n* value) located between the 2D-planes in an attempt to get closer to that of the 3D,[21,22] but at the expense of stability, contrary to the initial objective. The latter, on the contrary, promotes a specific crystallographic orientation of the 2D planes, perpendicular to the electrodes, providing a fluent and fast charge transport channel along the carrier

collection direction. This option has demonstrated remarkable results during the past few years, applied to an extended variety of 2D perovskite compositions.[10,23-25] Among them, the hot-casting technique was the first employed to report preferential out-of-plane crystal alignment in BA-based 2D perovskites.[10] Similarly, by lowering the precursor saturation in the perovskite solution, vertically oriented BA- and PEA- 2D systems have been successfully formed, mostly based on the precise tuning of the organic spacers and/or mix of solvents.[24] Unfortunately, even so these strategies facilitated a more efficient charge extraction, they also increased the complexity of the process, as they require strict conditions to precisely control the substrate temperature and compositions. Recently, an easier approach incorporating functional additives into the perovskite has demonstrated effective control on the crystal growth, providing a potential simple method to promote crystal orientation. Among the different candidates, DMSO, NH_4SCN and MACl have successfully induced highly oriented PEA-, BA-, and 2-thiophenemethylammonium (ThMA)-based 2D perovskites, allowing cell efficiencies over 13%.[26-29] These performances are however far below the state-of-the-art systems. In addition, despite the many options reported so far, most of the improvements observed in literature have been driven by the arbitrary use of large ammonium cations. There is still a lack of understanding about the crystal growth in 2D perovskites and the universal interactions ruling the crystal orientation, which is necessary for developing easy-to-operate and reproducible approaches to allow further improvements in device efficiency.

In this contribution, we present a simple and universal approach through rotating the crystallographic orientation perpendicular to the electrodes to boost the efficiency of PSCs based on LDRP and LDDJ perovskites. By using specific functional additives, and their synergistic effect with water molecules, we can precisely control the crystallographic orientation on a variety of 2D perovskites, including BA-, PEA-, and 1-naphthylmethylamine (NMA)-based LDRP perovskites, as well as butane diamine (BDA)-, 1,4-phenylenediamine (PDA)-based LDDJ perovskites. The mechanism ruling crystal rotation was investigated by comparing a series of active ammonium halides

incorporated into the system. Our results reveal that the specific adsorption of NH_4Cl to the (202) crystal plane, combined with its high volatility, promotes an out-of-plane crystal alignment during the film formation, further facilitated by the fast deprotonation of NH_4^+ induced by H_2O. This growing mechanism, supported by density functional theory (DFT) calculations, results in 2D perovskites with enhanced crystallinity, increased carrier mobility and prolonged carrier lifetimes by orders of magnitude, thanks to the vertical orientation and a notable decrease in the density of trap states. As a representative, planar solar cells containing $(PEA)_2(MA)_3Pb_4I_{13}$ exhibited an efficiency as high as 17.03%, which is among the records reported for 2D ($n \leq 4$) PSCs, and more importantly, a remarkable stability against moisture and temperature. Our strategy, named hereafter vertically-rotated (VR) methodology, elucidates the mechanism behind crystal-aligning additives, providing new insights for their proper selection and universal guidelines to realize highly efficient and stable low-dimensional PSCs.

Results and discussion

The $(PEA)_2(MA)_3Pb_4I_{13}$ was used as the representative 2D perovskite in the current study since it has prominent stability due to the hydrophobic benzene ring. Five ammonium salts consisting of 12.5 mol% NH_4I, NH_4Br, NH_4Cl, MACl, and PEACl were selected as additives to induce the VR-mechanism, based on the consideration that they can interact with perovskite framework and easily escape from the film.[30,31] The cells were prepared through a simple one-step solution process, that is, without any hot-casting or further steps like in the antisolvent method. Fig. 1a and Fig. S1 (ESI†) presents the cross-sectional and surface scanning electron microscopy (SEM) images of these samples, respectively. Densely packed perovskite crystals are observed in all samples, and the layer thickness is around 360 nm, which allows a well-balanced light absorption and charge transport.[32] Large-sized and even column-like (the NH_4Cl and NH_4Br sample) crystalline grains in the vertical direction were identified for the perovskite films containing additives, indicating less grain boundaries and

recombination centers. In addition, all perovskite films exhibit very homogeneous and continuous surface coverage, except for those containing NH_4I and PEACl additives, which show some cracks on the surface.

To gain insight into the crystal arrangement and orientation of the films, we performed X-ray diffraction (XRD) measurement. The perovskite films exhibit two dominant peaks located at around 14.2° and 28.5° (Fig. 1b, c), corresponding to the (111) and (202) crystal planes of quasi-2D perovskites, respectively.[10,14] Compared to the pristine material, the additives promote enhanced crystallinity, as suggested by the strengthening of peak intensity by 10 to 20 times and narrowing of the full width at half-maximum (FWHM) from ~ 0.45° to ~ 0.15° in (111) crystal plane. Observing the results, an increased peak intensity and decreased FWHM are obtained for NH_4^+ compared to MA^+ and PEA^+, similarly to changing I^- and Br^- for Cl^-. According to the Scherrer equation, the decreased FWHM suggests the increased grain size of perovskite film with NH_4Cl. These results suggest the formation of a large-sized crystal grain and a highly-oriented crystal structure using NH_4Cl. The absence of low-angle diffraction peaks corresponding to (0k0) planes,[32,33] which are related to perovskite crystals (small n) grown parallel to the substrate, indicates a high possibility of vertically oriented 2D perovskite crystals. Therefore, NH_4Cl could be a good option for the VR method, and could plausibly enhance the device performance of 2D perovskite systems.

To verify the applicability of these materials, we embodied the perovskites into planar p-i-n devices with the configuration of FTO/PEDOT:PSS/$(PEA)_2(MA)_3Pb_4I_{13}$/$PC_{61}BM$/BCP/Ag. Fig. 1d shows the current density-voltage (*J-V*) characteristics for the systems discussed above (see ESI,† Fig. S2 and Table S1). In particular, we highlight that the short-circuit current densities (J_{SC}) are remarkably improved when the additives are incorporated. Because differences in the absorption properties of $(PEA)_2(MA)_3Pb_4I_{13}$ films after the addition of additives (see ESI,† Fig. S3) are very minor, the improvement of J_{SC} may derive from an enhanced vertical orientation. Note that among all additives, devices containing NH_4Cl provide the best performance. We further optimized the concentration of NH_4Cl additive (*x* value in PEAI: MAI: PbI_2:

NH_4Cl = 2: 3: 4: x) as depicted in Fig. 1e (see ESI,† Table S1), and the best efficiency was found for x = 0.5. An acceptable efficiency of 13.34% is realized (J_{SC} of 14.49 mA/cm2, open-circuit voltage (V_{OC}) of 1.17 V and fill factor (FF) of 78.66%), which is significantly higher than that obtained for the reference device 0.59% (J_{SC} = 0.94 mA/cm2, V_{OC} = 1.01 V and FF = 62.27%), in agreement with previous reports.[27,28]

To investigate the reason for the enhanced device performance, we analyzed the crystallographic structure by grazing-incidence wide-angle X-ray scattering (GIWAXS). The GIWAXS images of the 2D and VR-2D $(PEA)_2(MA)_3Pb_4I_{13}$ films are shown in Fig. 1f, g. The main peaks which are indexed as (111) and (202) crystal planes for 2D perovskites match the dominant peaks at ~14.2° and ~28.5° appearing in normal XRD patterns. Note that the reflection of (202) plane along q_z is not fully recorded due to the detector limitation and more complete diffraction are identified in the 2D XRD image (Figure 3e). The reference 2D perovskite film displays less orientation with combined features of Debye-Scherrer arcs and partial scattered spots, compared to the sharper and stronger Bragg spots with obvious features of discrete spots at the same q positions for the VR-2D film.[10,34] By indexing the Bragg spots in Fig. 1h, we prove that the crystalline domains of VR-2D perovskite are rotated with their (202) planes parallel to the substrate, which leads to the inorganic framework perpendicularly aligned to it, contrary to the multidirectional crystallization in the reference film. These results demonstrate higher degree of out-of-plane orientation promoted by NH_4Cl,[28,35] consistent with the XRD results. Such crystal rotation, induced by the additive, suppresses the energy barrier typically associated with the insulating organic cations, enabling efficient charge-transport to the electrodes along the inorganic planes.[13,28,35]

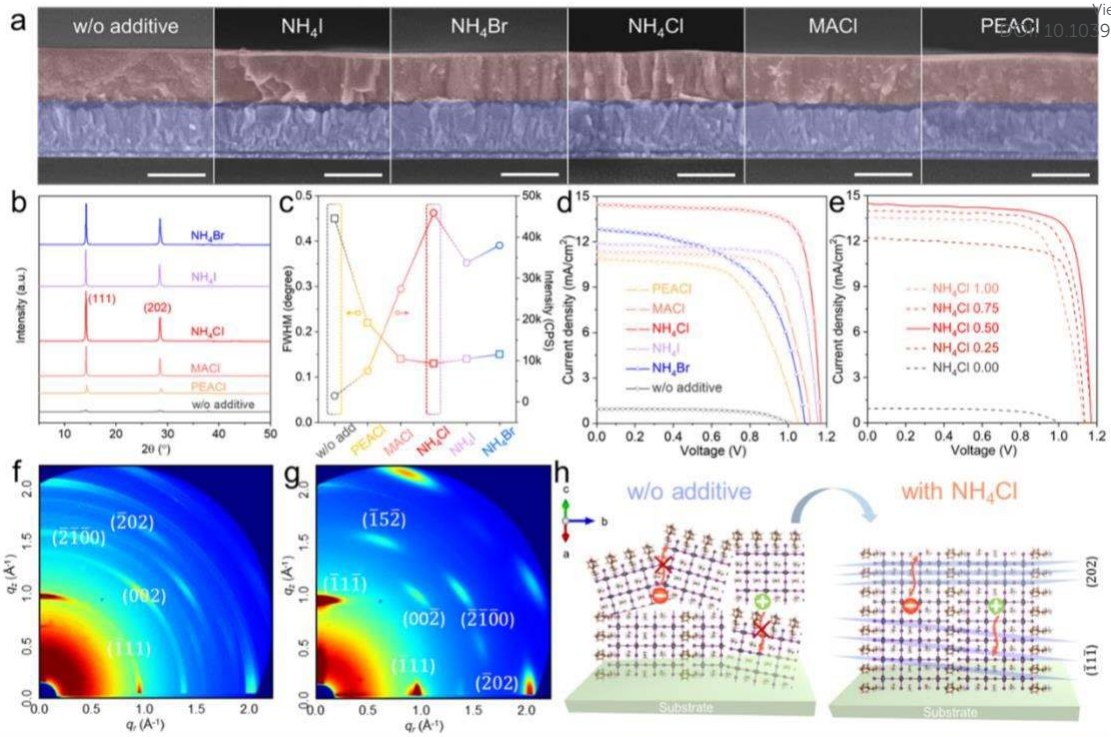

Fig. 1. (a) Cross-sectional SEM images of the $(PEA)_2(MA)_3Pb_4I_{13}$ films without/with additives, scale bars, 400 nm. (b) XRD patterns of $(PEA)_2(MA)_3Pb_4I_{13}$ films with different additives. (c) Comparison of FWHM and intensity of the (111) peak for different films. The circles represent the peak intensity and the squares represent the FWHM. (d) The *J-V* characteristics of 2D PSCs with different additives. (e) Device performance with various NH_4Cl concentrations. GIWAXS patterns for polycrystalline 2D (f) and VR-2D (g) $(PEA)_2(MA)_3Pb_4I_{13}$ perovskite films with colour scale proportional to the scattering intensity and Miller indices of the prominent peaks. The incidence angle is 0.2°. (h) Schematic representation of the 2D perovskite crystal structures without/with NH_4Cl.

To shed light on the crystallization mechanism, we performed DFT calculations in order to estimate the adsorption energies (E_{ads}) (relative to those of PEA^+) for NH_4^+ and MA^+ on the exposed (111) and (202) crystal planes with both PbI_2-terminated and MAI-terminated surfaces (Fig. 2a). The E_{ads} of NH_4^+ species is defined by $E_{ads} = E_{slab+cationic\ molecule\ adsorbed} - E_{slab} - E_{cationic\ molecule}$, where $E_{slab+cationic\ molecule\ adsorbed}$ represents the total energy of the adsorbed cationic molecules with the slab, E_{slab} is the total energy of the bare slab, and $E_{cationic\ molecule}$ is the energy of the isolated cationic molecule in a large

View Article Online
DOI: 10.1039/D0EE01833C

supercell. The adsorption energies were calculated considering the cationic molecules in gas phase, so the absolute values are not to be considered but their relative values between different cations and different surfaces and terminations are meaningful. As shown in Table S2, the NH_4^+ always shows higher adsorption energy than MA^+, irrespective of surfaces and terminations, indicating a preferential adsorption compared to MA^+, which may account for the unique advantage of NH_4^+ on regulating the 2D perovskite orientation. The surface formation energies (SFE) also reveals that the MAI-terminated (202) surface is the most stable surface which has the lowest SFE of 0.35 eV/nm^2 and NH_4^+ adsorbs more strongly than MA^+ on this surface, confirming a remarkable affinity of NH_4^+ to the MAI-terminated (202) surface. Note that the series of additives tested in this work could affect the crystallization differently according to different sizes of cations, types of halogens involved, as well as other material properties like, for example, the equilibrium vapor pressure. Indeed, these additives exhibit very different boiling points, and this might be crucial for crystal formation and growth. By analyzing *i)* the impact on device performance, *ii)* the boiling point values for each additive, *iii)* combined with the DFT calculations, we speculate that the mechanism enabling NH_4Cl to control the 2D crystal orientation must relate to its easy evaporation combined to the preferential adsorption on the (202) crystal plane. We rationalize the process as follows: different from the conventional perovskite formation (Fig. 2b), NH_4Cl molecules will mostly interact with $(PEA)_2(MA)_3Pb_4I_{13}$ particles through the (202) crystal planes (Fig. 2c) at the initial stages of perovskite crystallization. With the subsequent annealing of the system, NH_4Cl will gradually escape, leveling the (202) crystal plane on account of the normal-oriented evaporation. Meanwhile, PEA^+ will spontaneously occupy the positions perpendicular to these planes and complete the perovskite crystallization. This process results in the longitudinal growth of the inorganic slabs, leading to a highly oriented perovskite film. Note that we additionally verified the film composition by depth profile X-ray photoelectron spectroscopy (XPS), and no presence of Cl after crystallization could be detected, neither in the perovskite bulk nor at the interface (see ESI,† Fig. S4). Because

Cl has been previously associated to the formation of highly oriented crystals, we further replaced NH_{4+} by a less volatile K_+ cation, in order to exclusively target the effect of Cl in our films. With that purposed we prepared films containing KCl in either the PEDOT:PSS/perovskite interface or within the perovskite bulk. The crystallographic characterization of these systems, shown in Fig. S5 (ESI†), revealed no influence on the XRD patterns induced by KCl interlayer, and a small contribution (very minor compared to that obtained for NH_4Cl) of out-of-plane crystal growth for KCl added to the bulk, plausibly due to the promoted evaporation of partial MA_+ in terms of MACl during film formation. Therefore, the preferential orientation which is exclusively induced by Cl is very limited, and does not directly regulate the crystallization/orientation in the VR method, but it rather promotes the evaporation of NH_{4+}, inducing the out-of-plane orientation during film formation.

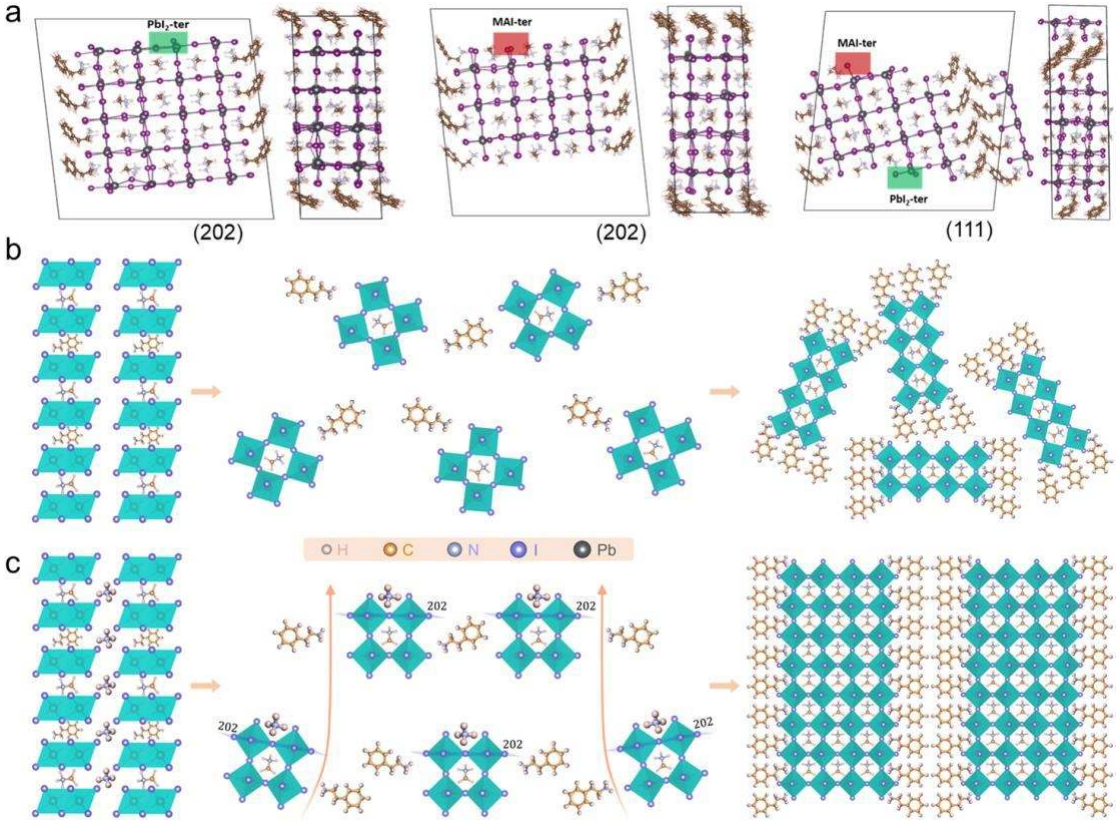

Fig. 2. (a) Optimized structures of (202) and (111) surfaces with both PbI_2- and MAI-termination. Highlighted region shows the adsorption sites where molecular species are adsorbed. (c) The schematic diagram for the random crystallization of $(PEA)_2(MA)_3Pb_4I_{13}$ in the conventional method. (g) The schematic diagram for the

View Article Online
DOI: 10.1039/D0EE01833C

proposed mechanism of the vertical orientation, showing the flattened (202) crystal plane caused by the NH_4Cl evaporation.

If the above mechanism were correct, some parameters affecting NH_4Cl would have a strong impact on the crystal growth dynamics. For example, it is well known that H_2O can easily deprotonate ammonium species, forming ammonia and hydrogen chloride in their gas phase according to the Grotthuss mechanism.[30,36] Given that NH_4^+ evaporation rules the VR process, such deprotonation would promote the volatilization of the additive until its complete depletion, therefore enhancing the growth of the perovskite towards the 2D vertical planes. This synergic effect, previously reported in the literature for $MAPbI_3$, could have paramount significance for the realization of high-efficiency 2D perovskite systems, paving the way towards stable and efficient devices. To verify this idea, we directly incorporated H_2O into the perovskite precursor and deposited $(PEA)_2(MA)_3Pb_4I_{13}$ perovskite films. Interestingly, cross-sectional SEM images suggest an obviously enhanced crystal growth in the vertical direction when H_2O was introduced (see ESI,† Fig. S6a). Despite some pinholes appear on the film surface for H_2O exceeding 1 vol % (see ESI,† Fig. S6b), the films are compact with H_2O contents below these values. This is also reflected in device performance, which shows increasing J_{SC} from 14.27 mA/cm2 to 18.16 mA/cm2 for 1 vol % H_2O addition (see ESI,† Fig. S7 and Table S1), while larger percent of H_2O (between 1.5 and 2 vol %) causes degradation (J_{SC} slightly declines, together with V_{OC} and FF). As a result, PCE only improves from 13.02% to 14.61% when $H_2O \leq 1$ vol %.

To soften such adverse effects, a more moderate incorporation of H_2O was introduced *via* tuning the environmental relative humidity (RH) from 10% to 50%. As expected from previous results, increasing the ambient moisture strengthens the longitudinal growth of 2D perovskite with dense and large grains (Fig. 3a). Indeed, despite highly humid environments tend to induce the formation of pinholes (> 40% RH, see ESI,† Fig. S8), a better control on the perovskite morphology could be achieved for lower RH values. Consequently, enhanced morphology, preferred vertical orientation (see ESI,† Fig. S9a) and optimal device performance was achieved under

30% RH (Fig. 3b and see ESI,† Table S1). We further analyzed the composition of these perovskite films with ion chromatography (IC) technique. The amounts of NH_4^+ residues remaining in the films were evaluated as presented in Fig. 3c, where the signal of Na^+ comes from the solvent of the IC measurement. The results confirm that those films prepared in higher RH % contain less residual NH_4^+, suggesting the preferential deprotonation of NH_4^+ promoted by H_2O.

To broaden the perspective of our observations and to demonstrate the universality of the VR strategy, five typical 2D perovskites were fabricated under 30% RH (Fig. 3d), including LDRP systems [$(BA)_2MA_3Pb_4I_{13}$, $(PEA)_2MA_3Pb_4I_{13}$ and $(NMA)_2MA_3Pb_4I_{13}$], as well as LDDJ systems [$(BDA)MA_3Pb_4I_{13}$ and $(PDA)MA_3Pb_4I_{13}$]. As observed in Fig. 3e, the strong and discrete Bragg spots in all grazing incidence 2D XRD images demonstrate the preferred vertical orientation for either LDRP or LDDJ perovskites, with the independence of the cation types. The diffraction rings covering the whole detector are from the fluorine-doped tin oxide (FTO) substrate (see ESI,† Fig. S9b). Additionally, significant improvements in PCEs were observed owing to a remarkably increased J_{SC} (see ESI,† Fig. S10). Therefore, using the synergistic effect of NH_4Cl and H_2O is certified as an effective and universal approach to rotate the 2D perovskite orientation and enhance the photovoltaic performance of 2D PSCs.

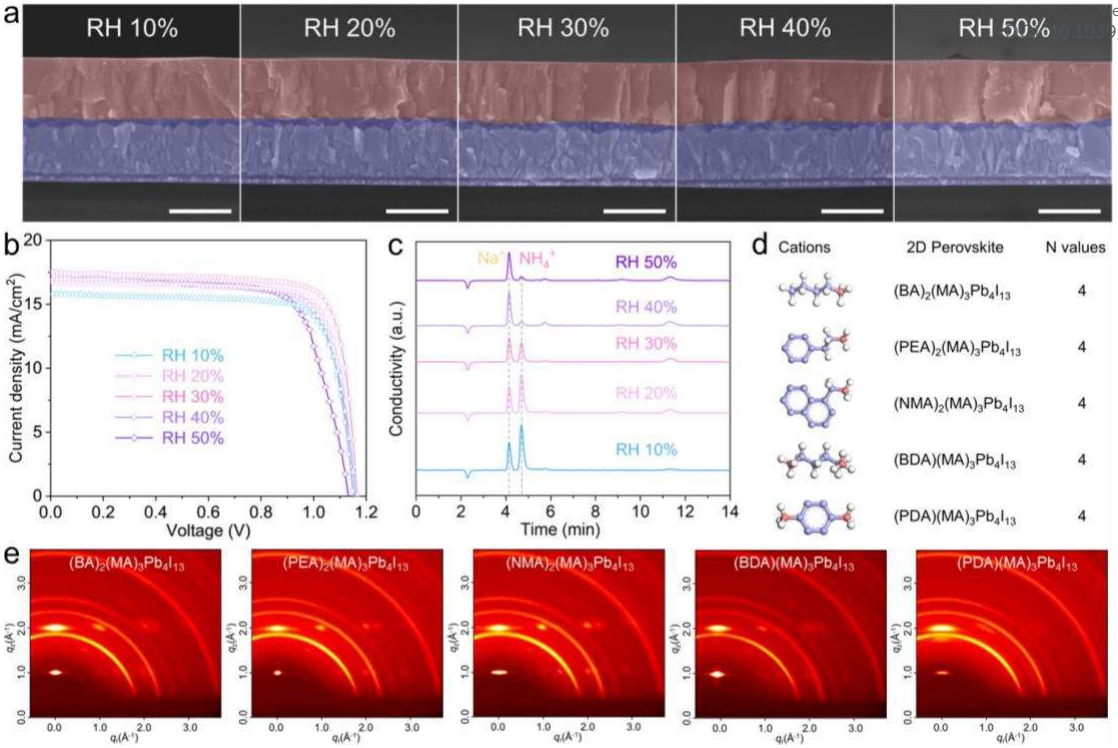

Fig. 3. (a) Cross-sectional SEM images, scale bars, 400 nm. (b) *J-V* characteristics of VR-2D $(PEA)_2(MA)_3Pb_4I_{13}$ PSCs fabricated under different ambient humidities. (c) IC spectra of VR-2D $(PEA)_2(MA)_3Pb_4I_{13}$ films fabricated under different ambient humidities. (d) Molecule formula of five typical 2D perovskites with different spacing cations. (e) 2D XRD images of five typical 2D perovskite films using the VR strategy.

Moreover, thanks to the VR method, the $(PEA)_2(MA)_3Pb_4I_{13}$ perovskite film exhibited brand new characteristics, especially for the charge transport properties. To investigate the impact on the mobility of photogenerated carriers, we analyzed the space-charge limited currents (SCLC) for VR-2D perovskite semiconductors. Electron-only and hole-only semiconductor devices were fabricated with the architecture FTO/TiO_2/$(PEA)_2(MA)_3Pb_4I_{13}$/$PC_{60}BM$/Ag and FTO/PEDOT:PSS/ $(PEA)_2(MA)_3Pb_4I_{13}$/PTAA/Au, respectively. The dark *J-V* characteristics, shown in Fig. 4a and Fig. S11a (ESI†), demonstrate that both the electron- and hole-mobilities (μ_e, μ_h respectively) are remarkably improved by 2 to 3 orders of magnitude, as expected from a more efficient charge-transport due to aligned crystallinity (Fig. 1h). The VR-2D perovskite exhibits increased carrier mobilities, especially the hole mobility, compared to other reported values (see ESI,† Table S3). The much closer μ_h and μ_e values also

demonstrate an almost balanced charge carrier transport (Table 1). In addition, we also quantified the trap densities of the 2D and VR-2D $(PEA)_2(MA)_3Pb_4I_{13}$ films. The three regions including the ohmic response, SCLC response and trap-filled limited response in Fig. 4b, indicate that the trap density has been reduced by 1 order of magnitude (Table 1), attributed to the perfectly rotated crystal orientation.

To further demonstrate this mechanism, we monitored the time-resolved photoluminescence (TRPL) and steady-state PL of the perovskites deposited on FTO/PEDOT:PSS substrates. The PL-decay for all samples is dominated by a fast (τ_1) and slow (τ_2) decay components, corresponding to the quenching of free carriers at the perovskite/PEDOT:PSS interface and radiative decay, respectively (Table S4).[37-39] Comparing both systems, we verify enhanced charge extraction and transfer for the VR method (Fig. 4c). In this case, the τ_1 is decreased while its weight fraction is increased, confirming a more facilitated transfer of photogenerated free carriers, and a higher contribution to the decay process. A significant PL quenching was also observed for the vertically oriented film, related to a more efficient hole transfer to the substrate (Fig. 4d).[27,40] To gain insight into the film distribution in the micrometer scale, we analyzed the film homogeneity in 2D and VR-2D perovskites with micro-PL spectroscopy. Averaged over a diffraction-limited spot size of 0.16 μm^2, this technique provides valuable information about local heterogeneities, intimately linked to crystal defects and charge extractions. Fig. 4e and f show the map of the PL peak intensity (from 675 to 825 nm) distributed over 10 × 10 μm^2 areas. A more homogeneous PL distribution and a lower integrated intensity for the VR-2D films were detected. Overall, the results suggest suppressed defects, facilitated charge extraction and carrier transport to the HTL layer, which is plausibly the reason for obtaining enhanced J_{SC} and FF for these 2D PSCs.

View Article Online
DOI: 10.1039/D0EE01833C

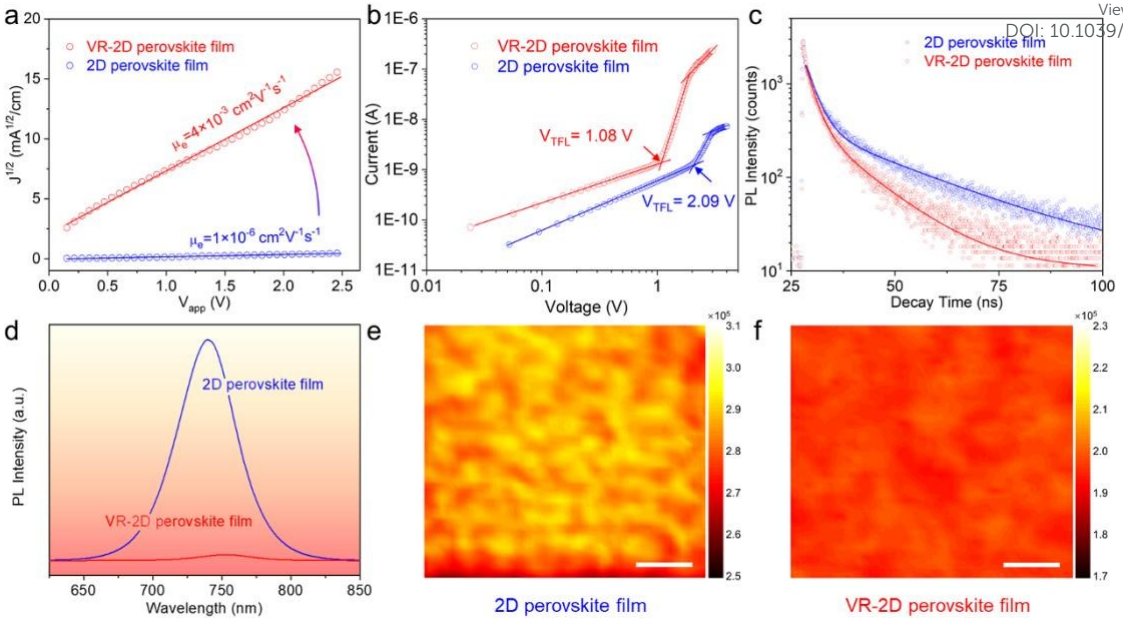

Fig. 4. (a) Dark *J-V* curves for the electron-only devices. (b) SCLC curves showing the typical three regions. (c) PL decay curves and (d) PL curves for the 2D and VR-2D $(PEA)_2(MA)_3Pb_4I_{13}$ films. PL mapping intensity integrated from 675 to 825 nm of the (e) 2D and (f) VR-2D film, scale bars, 2 μm.

Importantly, applying the optimal conditions to VR-2D $(PEA)_2(MA)_3Pb_4I_{13}$ perovskite (n = 4), a device efficiency as high as 17.03% was obtained (J_{SC} of 18.47 mA·cm^{-2}, V_{OC} of 1.17 V and FF of 79.13%), which also exhibited negligible photocurrent hysteresis (Fig. 5a). The incident photon-to-current conversion efficiency (IPCE), shown in Fig. 5b, demonstrates an integrated photocurrent closely matching the J_{SC} value extracted from the *J-V* characteristic. As previously asserted, we attribute the high current density to the ideal vertical orientation induced by the synergistic effect of NH_4Cl and H_2O. To verify this, we analyzed the carrier transport and transfer by electrochemical impedance spectroscopy (EIS) measurement.[41] Nyquist plots of the devices in Fig. S11b (ESI†) were measured under dark conditions by applying a bias of 0.8V. The fitted series resistance (R_S) and charge transfer resistance (R_{CT}) for the $(PEA)_2(MA)_3Pb_4I_{13}$-based device are 10.63 Ω and 289.40 Ω, respectively. A clear smaller R_S of 7.20 Ω and R_{CT} of 131.06 Ω are observed when VR method is introduced, indicating enhanced carrier transport and better carrier extraction, consistent with the

SCLC and TRPL results. Fig. 5c depicts the natural logarithmic relationship between light intensity and V_{OC}, which can provide critical information on the recombination processes.[39] The light-dependent V_{OC} gives a slope of $n\,kT/q$, which defines the ideality factor. A slope of 2 kT/q predicts the occurrence of trap-assisted recombination, while a slope of kT/q denotes a trap-free condition.[39] In perfect agreement, the slope of V_{OC} versus light intensity decreases from 1.99 kT/q to 1.56 kT/q after using the VR method, confirming that trap-assisted charge recombination is effectively mitigated.[7] We also evaluated the carrier recombination dynamics through the transient photovoltage decay (TPV) (Fig. 5d), which shows a 10-fold increase (4.24 ms) in charge recombination lifetime for the VR-based device compared to 0.41 ms for the reference device. This behavior confirms that the charge recombination losses are significantly lowered.

Finally, the long-term stability of our VR-2D $(PEA)_2(MA)_3Pb_4I_{13}$ films and the typical 3D $MAPbI_3$ were simultaneously investigated. We first tested the stability via XRD, by storing the samples under ambient air at 25ºC with RH of ~ 40%. As shown in Fig. S12a and 12b (ESI†), the VR-2D systems do not show any PbI_2 peak (~12.6°) after 150 days, contrary to the 3D $MAPbI_3$ in which an obvious signal appears after ~60 days. This remarkable improvement is attributed to the stronger tolerance of 2D perovskite against moisture.[17] Consequently, a remarkable stability was obtained for non-encapsulated devices based on 2D perovskite, as shown in Fig. 5e. Then, we further compared the thermal stability of the 2D and 3D perovskites under continuous heating at 85 ºC. Fig. S12c and 12d (ESI†) present the XRD patterns of both systems, evidencing the enhanced resistance of 2D perovskites compared to the 3D. Similarly, non-encapsulated devices containing the 2D perovskite were also evaluated at 85ºC in an inert atmosphere, which maintained over 90% of the initial efficiency after 1600 h of aging (Fig. 5f). Such robust stability represents a major progress in PSCs, as it allows improved environmental tolerance against moisture and heat for 2D PSCs, together with improved efficiency.[14,32,42] More importantly, the PSC stability can be further enhanced by chemical approaches[43] as well as nitrogen soaking,[44] represinting a bright for their future commercialization.

View Article Online
DOI: 10.1039/D0EE01833C

Table 1. The electron mobility (μ_e), hole mobility (μ_h) and trap densities (N_t) of the 2D perovskite films and series resistance (R_S), charge transfer resistance (R_{CT}), ideality factor (n) and carrier recombination lifetime (τ) for the 2D PSCs.

Samples	μ_e ($cm^2V^{-1}s^{-1}$)	μ_h ($cm^2V^{-1}s^{-1}$)	μ_h/μ_e	R_S (Ω)	R_{CT} (Ω)	N_t (cm^{-3})	n	τ (ms)
2D	1.43×10^{-6}	4.41×10^{-5}	31	10.63	289.40	1.59×10^{16}	1.99	0.41
VR-2D	3.56×10^{-3}	7.20×10^{-3}	2	7.20	131.06	3.73×10^{15}	1.56	4.24

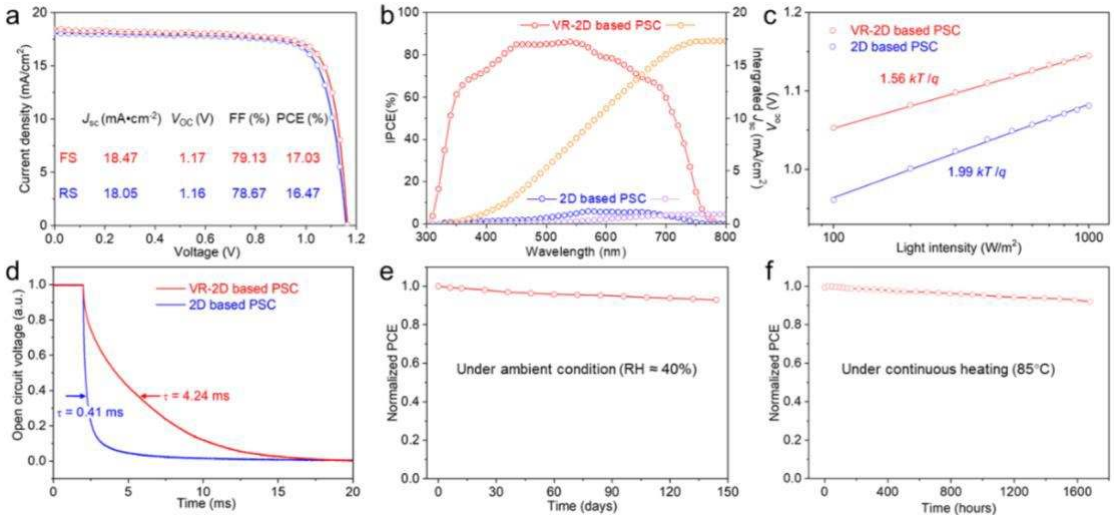

Fig. 5. (a) *J-V* characteristics of the champion device. (b) IPCE curves and the integrated J_{SC} of typical 2D PSCs. (c) Light-dependent V_{OC} and (d) normalized transient photovoltage decay curves of the 2D and VR-2D perovskite solar cells. (e) PCE evaluation of the VR-2D device under 40% RH at 25℃ in dark. (f) PCE evaluation of the VR-2D device at 85℃ in N_2.

Conclusions

In summary, a VR strategy has been successfully established to universally improve the PCEs of 2D PSCs. The orientation control of 2D perovskites and the corresponding crystallization mechanism has been systematically investigated by employing a series of active additives and the assistance of DFT calculations. The enhanced crystallinity, improved charge transport, and extended carrier lifetime, as well as effectively subdued

non-radiative carrier recombination and reduced trap densities, were obtained by the synergistic effect of NH_4Cl additive and H_2O inducer. The excellent structural, crystallographic and optoelectrical properties yielded a dramatic improvement of PCE from 0.59% to 17.03% as well as superb long-term environmental stability. Our findings indicate a promising future of efficient and stable low-dimensional PSCs by implementing the VR approach.

Conflict of Interest

There are no conflicts to declare.

Acknowledgments

The authors acknowledge support from the National Natural Science Foundation of China (Nos. U1705256 and 51702096), the 111 Project (No. B16016), the Fundamental Research Funds for the Central Universities (No. 2017MS021) and the PhD scholarship from China Scholarship Council (Grant Nos. 201506060156, 201906730051 and 201906730050). The authors appreciate the Beijing Synchrotron Radiation Facility for providing technical support.

References

1. D. Bi, W. Tress, M. I. Dar, P. Gao, J. Luo, C. Renevier, K. Schenk, A. Abate, F. Giordano and J. P. C. Baena, *Sci. Adv.*, 2016, **2**, e1501170-e1501170.
2. Q. Jiang, Y. Zhao, X. Zhang, X. Yang, Y. Chen, Z. Chu, Q. Ye, X. Li, Z. Yin and J. You, *Nature Photon.*, 2019, **13**, 460-466.
3. https://www.nrel.gov/pv/cell-efficiency.html, accessed on February 26, 2020.
4. S. Rühle, *Sol. Energy*, 2016, **130**, 139-147.
5. I. Deretzis, E. Smecca, G. Mannino, A. La Magna, T. Miyasaka and A. Alberti, *J. Phys. Chem. L.*, 2018, **9**, 3000-3007.
6. Y. Liu, Z. Hong, Q. Chen, H. Chen, W. H. Chang, Y. Yang, T. B. Song and Y. Yang, *Adv. Mater.*, 2016, **28**, 440-446.

7. Y. Yang, C. Liu, Y. Ding, Z. Arain, S. Wang, X. Liu, T. Hayat, A. Alsaedi and S. Dai, *ACS Appl. Mater. Interfaces*, 2019, **11**, 34964-34972.
8. R. Wang, J. Xue, K.-L. Wang, Z.-K. Wang, Y. Luo, D. Fenning, G. Xu, S. Nuryyeva, T. Huang and Y. Zhao, *Science*, 2019, **366**, 1509-1513.
9. C. Liu, Y. Yang, X. Xia, Y. Ding, Z. Arain, S. An, X. Liu, R. C. Cristina, S. Dai and M. K. Nazeeruddin, *Adv. Energy Mater.*, 2020, 1903751.
10. H. Tsai, W. Nie, J.-C. Blancon, C. C. Stoumpos, R. Asadpour, B. Harutyunyan, A. J. Neukirch, R. Verduzco, J. J. Crochet and S. Tretiak, *Nature*, 2016, **536**, 312.
11. Y. Li, J. V. Milić, A. Ummadisingu, J.-Y. Seo, J.-H. Im, H.-S. Kim, Y. Liu, M. I. Dar, S. M. Zakeeruddin and P. Wang, *Nano Lett.*, 2018, **19**, 150-157.
12. X. Zhang, X. Ren, B. Liu, R. Munir, X. Zhu, D. Yang, J. Li, Y. Liu, D.-M. Smilgies and R. Li, *Energy Environ. Sci.*, 2017, **10**, 2095-2102.
13. H. Pan, X. Zhao, X. Gong, Y. Shen and M. Wang, *J Phys. Chem. Lett.*, 2019, **10**, 1813-1819.
14. S. Chen, N. Shen, L. Zhang, W. Kong, L. Zhang, C. Cheng and B. Xu, *J. Mater. Chem. A*, 2019, **7**, 9542-9549.
15. L. Mao, W. Ke, L. Pedesseau, Y. Wu, C. Katan, J. Even, M. R. Wasielewski, C. C. Stoumpos and M. G. Kanatzidis, *J. Am. Chem. Soc.*, 2018, **140**, 3775-3783.
16. L. N. Quan, M. Yuan, R. Comin, O. Voznyy, E. M. Beauregard, S. Hoogland, A. Buin, A. R. Kirmani, K. Zhao and A. Amassian, *J. Am. Chem. Soc.*, 2016, **138**, 2649-2655.
17. D. Thrithamarassery Gangadharan and D. Ma, *Energy Environ. Sci.*, 2019, **12**, 2860-2889.
18. Y. Chen, Y. Sun, J. Peng, J. Tang, K. Zheng and Z. Liang, *Adv. Mater.*, 2018, **30**, 1703487.
19. J. Even, L. Pedesseau and C. Katan, *ChemPhysChem*, 2014, **15**, 3733-3741.
20. P. Li, C. Liang, X. L. Liu, F. Li, Y. Zhang, X. T. Liu, H. Gu, X. Hu, G. Xing and X. Tao, *Adv. Mater.*, 2019, **31**, 1901966.

21. N. Li, Z. Zhu, C. C. Chueh, H. Liu, B. Peng, A. Petrone, X. Li, L. Wang and A. K. Y. Jen, *Adv. Energy Mater.*, 2017, **7**, 1601307.

22. H. Zheng, G. Liu, L. Zhu, J. Ye, X. Zhang, A. Alsaedi, T. Hayat, X. Pan and S. Dai, *Adv. Energy Mater.*, 2018, **8**, 1800051.

23. X. Zhang, G. Wu, S. Yang, W. Fu, Z. Zhang, C. Chen, W. Liu, J. Yan, W. Yang and H. Chen, *Small*, 2017, **13**, 1700611.

24. A. Z. Chen, M. Shiu, X. Deng, M. Mahmoud, D. Zhang, B. J. Foley, S.-H. Lee, G. Giri and J. J. Choi, *Chem. Mater.*, 2019, **31**, 1336-1343.

25. A. Z. Chen, M. Shiu, J. H. Ma, M. R. Alpert, D. Zhang, B. J. Foley, D.-M. Smilgies, S.-H. Lee and J. J. Choi, *Nat. Commun.*, 2018, **9**, 1-7.

26. L. Gao, F. Zhang, C. Xiao, X. Chen, B. W. Larson, J. J. Berry and K. Zhu, *Adv. Funct. Mater.*, 2019, 1901652.

27. X. Zhang, G. Wu, W. Fu, M. Qin, W. Yang, J. Yan, Z. Zhang, X. Lu and H. Chen, *Adv. Energy Mater.*, 2018, **8**, 1702498.

28. H. Lai, B. Kan, T. Liu, N. Zheng, Z. Xie, T. Zhou, X. Wan, X. Zhang, Y. Liu and Y. Chen, *J. Am. Chem. Soc.*, 2018, **140**, 11639-11646.

29. J. Wang, S. Luo, Y. Lin, Y. Chen, Y. Deng, Z. Li, K. Meng, G. Chen, T. Huang, S. Xiao, H. Huang, C. Zhou, L. Ding, J. He, J. Huang and Y. Yuan, *Nat. Commun.*, 2020, **11**, 582.

30. Y. Rong, X. Hou, Y. Hu, A. Mei, L. Liu, P. Wang and H. Han, *Nat. Commun.*, 2017, **8**, 14555.

31. H. Si, Q. Liao, Z. Kang, Y. Ou, J. Meng, Y. Liu, Z. Zhang and Y. Zhang, *Adv. Funct. Mater.*, 2017, **27**, 1701804.

32. J. Shi, Y. Gao, X. Gao, Y. Zhang, J. Zhang, X. Jing and M. Shao, *Adv. Mater.*, 2019, **31**, 1901673.

33. D. H. Cao, C. C. Stoumpos, O. K. Farha, J. T. Hupp and M. G. Kanatzidis, *J. Am. Chem. Soc.*, 2015, **137**, 7843-7850.

34. Y. Liu, S. Akin, L. Pan, R. Uchida, N. Arora, J. V. Milić, A. Hinderhofer, F. Schreiber, A. R. Uhl and S. M. Zakeeruddin, *Sci. Adv.*, 2019, **5**, eaaw2543.

35. J. Qing, X. K. Liu, M. Li, F. Liu, Z. Yuan, E. Tiukalova, Z. Yan, M. Duchamp, S. Chen and Y. Wang, *Adv. Energy Mater.*, 2018, **8**, 1800185.

36. H. Looyenga, *Physica*, 1965, **31**, 401-406.

37. C. Liu, M. Cai, Y. Yang, Z. Arain, Y. Ding, X. Shi, P. Shi, S. Ma, T. Hayat and A. Alsaedi, *J. Mater. Chem. A*, 2019, **7**, 11086-11094.

38. C. Liu, Y. Yang, O. A. Syzgantseva, Y. Ding, M. A. Syzgantseva, X. Zhang, A. M. Asiri, S. Dai and M. K. Nazeeruddin, *Adv. Mater.*, 2020, 2002632, DOI: 10.1002/adma.202002632.

39. Y. Yang, H. Peng, C. Liu, Z. Arain, Y. Ding, S. Ma, X. Liu, T. Hayat, A. Alsaedi and S. Dai, *J. Mater. Chem. A*, 2019, **7**, 6450-6458.

40. S. Yu, Y. Yan, Y. Chen, P. Chábera, K. Zheng and Z. Liang, *J. Mater. Chem. A*, 2019, **7**, 2015-2021.

41. D. Yang, X. Zhou, R. Yang, Z. Yang, W. Yu, X. Wang, C. Li, S. F. Liu and R. P. Chang, *Energy Environ. Sci.*, 2016, **9**, 3071-3078.

42. R. Yang, R. Li, Y. Cao, Y. Wei, Y. Miao, W. L. Tan, X. Jiao, H. Chen, L. Zhang, Q. Chen, H. Zhang, W. Zou, Y. Wang, M. Yang, C. Yi, N. Wang, F. Gao, C. R. McNeill, T. Qin, J. Wang and W. Huang, *Adv. Mater.*, 2018, **30**, 1804771.

43. J. W. Lee and N. G. Park, *Adv. Energy Mater.*, 2020, **10**, 1903249.

44. A. Alberti, I. Deretzis, G. Mannino, E. Smecca, F. Giannazzo, A. Listorti, S. Colella, S. Masi and A. La Magna, *Adv. Energy Mater.*, 2019, **9**, 1803450.

View Article Online
DOI: 10.1039/D0EE01833C

Broader context

Developing highly efficient two-dimensional (2D) perovskite solar cells (PSCs) with superior stability is inevitable for commercialization. At present, the performance of 2D PSCs is far behind that of 3D PSCs due to their strong exciton-binding energy and restrained charge transport. Although efforts on orientation control have been made to overcome this drawback, there is still a lack of general understanding about the oriented crystal growth and a universal method for further improving the performance of 2D PSCs. In this contribution, we design an effective and universal approach to enhance the 2D PSCs' efficiency by using the synergistic effect of ammonium chloride and water. The crystallographic orientation of 2D perovskites can be rotated perpendicularly to the electrodes, resulting in remarkably enhanced crystallinity, carrier mobilities, and carrier lifetimes by orders of magnitude. The resultant 2D PSC exhibits 17.03% efficiency, which is among the records reported for 2D ($n \leq 4$) PSCs, and more importantly, remarkable stability against moisture and temperature. This work elucidates the mechanism behind the aligned crystallization and provides a universal guideline to realize high-efficiency and stable low-dimensional PSCs.